



Breast Imaging Original Research

# Utility of Tissue Classification in Invasive Ductal Carcinoma using Dynamic Magnetic Resonance Imaging of the Mammary Gland

Yoshiaki Miyazaki<sup>1</sup>, Nobuyuki Tabata<sup>2</sup>, Yuichiro Kubo<sup>3</sup>, Kenji Shinozaki<sup>4</sup>

<sup>1</sup>Department of Radiological Technology, National Cancer Center, Tokyo, <sup>2</sup>Department of Radiology, National Hospital Organization Kyushu Medical Center, <sup>3</sup>Department of Clinical Radiology, Kyushu University Hospital, <sup>4</sup>Department of Radiology, National Hospital Organization Kyushu Cancer Center, Fukuoka, Japan.



\*Corresponding author:

Yoshiaki Miyazaki,  
Department of Radiological  
Technology, National Cancer  
Center, Tokyo, Japan.

[yomiyaza@ncc.go.jp](mailto:yomiyaza@ncc.go.jp)

Received : 20 September 2020

Accepted : 31 December 2020

Published : 18 January 2021

DOI

10.25259/JCIS\_173\_2020

Quick Response Code:



## ABSTRACT

**Objectives:** In Japan, invasive ductal carcinomas, which account for 75% of breast cancer cases, are sub-classified as solid, tubule-forming, scirrhous, and other types based on the histopathological findings. Although time-intensity curve (TIC) analysis of magnetic resonance (MR) images has shown diagnostic ability in differentiating benign and malignant tumors, its ability to diagnose different tumor tissue types has not yet been achieved. In this study, we report a histological classification of invasive ductal carcinoma using the TIC analysis of dynamic MR images of the mammary gland.

**Material and Methods:** A total of 312 invasive ductal carcinomas were analyzed, and each tissue type that indicated malignancy in the washout parts of the tumors was classified and characterized using the TIC.

**Results:** The tissue was classified, and the results were then compared to the pathohistological diagnosis. Using this method, the accuracy of tissue classification by quantitative analysis of TIC-MR images was 86.9% (271/312), which was higher than that obtained by ultrasonography 68.9% (215/312).

**Conclusion:** This method is effective for classifying tissue types in invasive ductal carcinoma.

**Keywords:** Breast cancer, Computer-aided diagnosis, Histological classification, Invasive ductal carcinoma, Time-intensity curve

## INTRODUCTION

Various tumors that occur in the mammary gland are histologically classified by the cell type, cytological findings, and histomorphological features. According to the Japanese Breast Cancer Society's "The General Rules for Clinical and Pathological Recording of Breast Cancer," invasive ductal carcinoma is considered to be malignant when the interstitium is infiltrated by the cancer cells.<sup>[1]</sup> Invasive ductal carcinoma is the most frequent malignancy of the mammary gland, accounting for more than 75% of all breast cancers,<sup>[2]</sup> and corresponds to the invasive carcinoma of no special type in the "World Health Organization (WHO) Classification of Tumors of the Breast" by the WHO.<sup>[3]</sup>

In addition, the 17<sup>th</sup> edition of "The General Rules for Clinical and Pathological Recording of Breast Cancer" classified invasive ductal carcinoma in Japan into solid-tubular, papillotubular,

This is an open-access article distributed under the terms of the Creative Commons Attribution-Non Commercial-Share Alike 4.0 License, which allows others to remix, tweak, and build upon the work non-commercially, as long as the author is credited and the new creations are licensed under the identical terms.

©2020 Published by Scientific Scholar on behalf of Journal of Clinical Imaging Science

and scirrhous carcinomas<sup>[4]</sup> with the ratio 1:1:2.<sup>[5]</sup> Three types of invasive ductal carcinoma in the tumor were mixed in various proportions.<sup>[6]</sup> Tissue morphology, degree of differentiation, degree of infiltration, or prognosis indirectly reflected this classification. The positive rate of lymph node metastasis and the infiltration of fatty tissue, lymphatic vessel invasion, and skin invasion of cancer increases in the order of papillotubular, solid-tubular, and scirrhous carcinomas. Therefore, the 10-year survival rate decreased in the order of papillary tubular cancer > solid-tubular cancer > scirrhous cancer.<sup>[6]</sup> This classification is the only one that takes into account inspection images such as ultrasounds as indicators in the mode of progression at the tumor site.<sup>[7,8]</sup> The new classification of invasive ductal carcinoma in the 18<sup>th</sup> edition of “The General Rules for Clinical and Pathological Recording of Breast Cancer” changed from solid-tubular carcinoma/papillotubular carcinoma (many tubules forming as a feature)/scirrhous carcinoma to solid types/tubule-forming types/scirrhous types/other types (when classification judgment is difficult or when an intermediate tissue image is shown).

Radiological evaluation of breast cancer using magnetic resonance imaging (MRI) has a very high detection rate in almost all cases except for special tumors (invasive lobular carcinoma, tubular carcinoma, cribriform carcinoma, mucinous carcinoma, carcinoma with apocrine differentiation) and microscopic lesions. The sensitivity is higher than that of mammography (68%) and ultrasonography (83%) and exceeds 95%.<sup>[9]</sup> Moreover, the high spatial resolution allows for an effective diagnosis (qualitative and spread) of breast tumors. The contrast enhancement effect of dynamic MRI examination reflects the blood flow condition in the tumor. Therefore, qualitative diagnosis can be expected from the analysis using the time-intensity curve (TIC) that plots the contrast enhancement effect of regions-of-interest over time<sup>[10]</sup> [Figure 1]. The diagnostic ability of TIC in differentiating between benign or malignant tumors has been proven.<sup>[11-18]</sup> However, as reported by Kamitani *et al.*, the ability of TIC to classify the histological type of breast cancer by tissue shape has unsatisfactory accuracy.<sup>[19]</sup> Hence, we extracted the TIC features of the invasive ductal carcinoma (solid, tubule-forming, scirrhous, and other types) and performed a histological classification based on the quantitative analysis results. Furthermore, we compared the accuracy of MRI-TIC to ultrasonography in classifying tissue based on the pathological diagnosis.

## MATERIAL AND METHODS

### Study design

A 1.5-Tesla MR device (Siemens Magnetom Symphony, Erlangen, Germany) was used with a 4-channel breast array

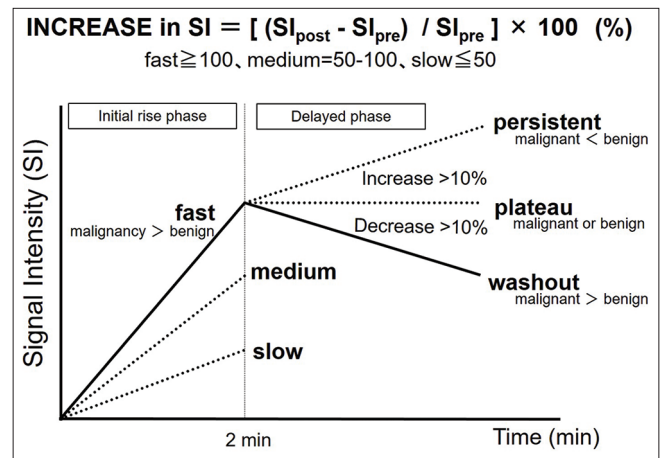


**Figure 1:** Overview of the time-intensity curve analysis.

coil to obtain a dynamic MR fat suppression T1-weighted image with the gadolinium contrast agent Magnevist IV (Schering Berlin, Germany) and the following parameters: Matrix size, 512 × 256; pixel size, 0.6 × 0.8 mm; slice thickness, 1.0 mm; TR, 5.42 s; TE, 2.11 s; flip angle, 20°; bandwidth of 300 Hz/pixel, with parallel imaging GeneRalized-Autocalibrating-Partial-Parallel-Acquisition (accel. factor PE: 2, ref. lines PE: 50), and the contrast medium injection device Sonic Shot GX (Nemoto Kyorindo co., Ltd, Tokyo, Japan). The contrast agent (0.2 ml/kg) was injected at a rate of 2.0 ml/s and 20 ml of physiological saline was boosted at a rate of 2.0 ml/s.

Dynamic MRI was performed in 4 phases: Before the injection of the contrast agent (pre-phase); immediately after the start of the contrast agent injection (injection phase); at 1 min (peak phase); and at 5 min (delay phase). The imaging time per phase was 1 min and the number of images per phase was 96 (384 total for all 4 phases). All 312 cases from April 2016 to March 2018 satisfied the following criteria: (1) Dynamic MRI performed, (2) no chemotherapy, and (3) definite diagnosis of invasive ductal carcinoma in the excised lesion. The patients were women aged 23–88 years (mean 57.9 ± 13.0 years) and had a tumor diameter between 0.7 and 9.2 cm (mean 2.4 ± 2.1 cm). Moreover, with the cooperation of a pathologist, we confirmed conformity to the new classification.<sup>[20]</sup>

In the clinical images in this study, all personal information was anonymized except for the MR images, pathological diagnosis names, and tumor location information. The ethics review committee of the management facility, the National Hospital Organization Kyushu Cancer Center (Approval No. 2016-52) approved the utilization of the data and waived the need for patient consent.

Figure 2 shows the method of tissue classification using TIC in the invasive ductal carcinomas. Using a total of 312 cases of

invasive ductal carcinoma of solid type (78), tubule-forming type (91), and scirrhous type (143), we investigated the washout effect part of the lesion that suggested malignancy. The method for extracting the washout effect area in the lesion is shown in Figure 3. Automatic extraction was used, as previously reported.<sup>[21]</sup>

One TIC was created for each pixel in the washout area in the lesion area of all the imaging slices. Next, the TIC for each pixel was summed up with the features of each tissue, and the tissue type with the most lesions was determined as the tissue type of the case. If there were multiple results of feature quantity aggregation, they were classified as “other.”

### Classification

The classification was determined using the TIC, based on the feature amount of each tissue type with  $\theta_1$  as the inclination angle of the change in the linear signal strength from the pre-phase to the injection phase with respect to the TIC time axis

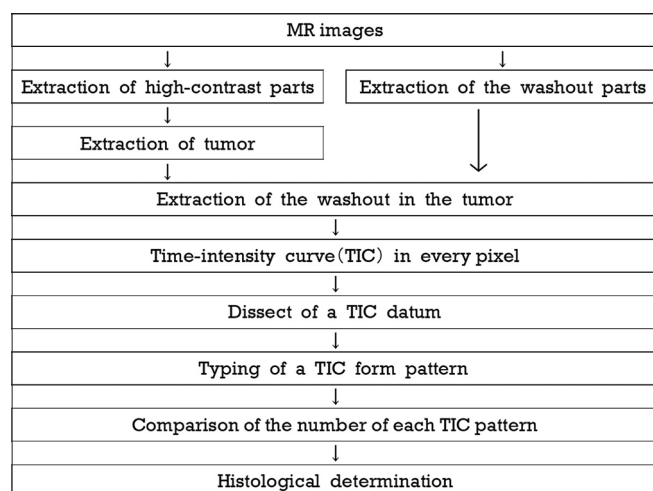


**Figure 2:** Flowchart of a histological classification method for invasive ductal carcinoma.

and  $\theta_2$  as the inclination angle of the linear signal strength from the injection phase to the peak phase [Figure 4].

Considering the difference in average peak time (time until the signal strength reached its peak), as reported by Kamitani *et al.* (the scirrhous type took the longest to reach the peak time),<sup>[19]</sup> the invasive ductal carcinoma was classified into solid, tubule-forming, scirrhous, and other types using the following formula (1).

$$\theta_1 \leq (k \times \theta_2), (k \times \theta_2) < \theta_1 \leq (j \times \theta_2), (j \times \theta_2) < \theta_1: \\ (0 < k < 1), (k < j) \quad (1)$$

The constant  $k$  increases by 0.01 and changes from 0.1 to  $j$ , whereas the constant  $j$  increases by 0.01 and changes from  $k$ . The constants  $k$  and  $j$  are values that show the cases where the TIC tissue classification and the pathological diagnosis most matched. A computer was used for the calculation and the transition of variable  $j$  to constant  $k$  and variable  $k$  to constant  $j$ .

### Statistical analysis

Analysis of variance (ANOVA) was performed on  $[\theta_2 - \theta_1]$  of the three classifications of data by TIC. All statistical analyses were performed with EZR (R Foundation for Statistical Computing, Vienna, Austria).<sup>[22]</sup> It is a modified version of the R commander designed to add statistical functions frequently used in biostatistics.

### Evaluation of TIC classification by comparing with pathological diagnosis after surgery

Sensitivity, specificity, positive predictive value, and negative reactive predictive value were calculated for each histological type for the TIC histological classification using the constants  $k$  and  $j$  obtained as described in section 2.2. In addition, the accuracy rate was calculated by the accuracy rate of the MRI-TIC test result and the ultrasonic test result.

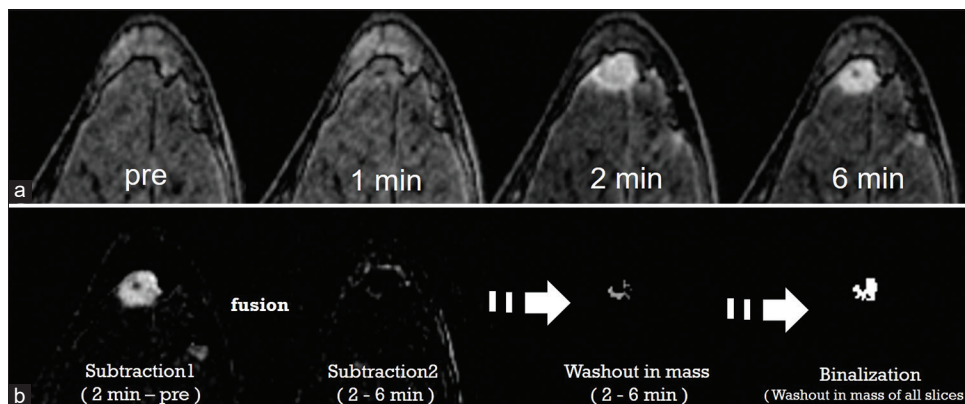


**Figure 3:** (a) Dynamic magnetic resonance imaging of a 42-year-old woman with left breast cancer (invasive ductal carcinoma in situ scirrhous type: 10 mm large mass) (b) processed images using a computer-aided diagnosis program in A.

## RESULTS

### Evaluation of features for each tissue type (determination of constants j and k)

TIC analysis showed washout in all 312 cases of invasive ductal carcinoma used in this study. Among the 312 cases, the k value was 0.54 and the j value was 0.97, which was the most consistent with the tissue classification using TIC and the pathological diagnosis. The transitions of the variable j at the constant k = 0.54 and the variable k at the constant j = 0.97 are shown in the graphs of Figures 5 and 6.

At j = 0.97 [Figure 5], the variable k value showed a sharp change in the matching rate around 0.4 between the tissue classification using TIC and pathological diagnosis. At k = 0.54 [Figure 6], the variable j has a constant value after j = 1.3, while drawing a mountain shape. The graph of Figure 7 shows the results of tissue classification using the formula (1), with k = 0.54 and j = 0.94, for each pathological tissue and the average value of  $\theta_1$  and  $\theta_2$  in the determined tissue.

Table 1 shows the results of the MRI-TIC tissue classification in comparison with the histopathological results. Seventy-eight cases had a pathological diagnosis of the solid type:  $(0.97 \times \theta_2) < \theta_1$  in 71/78 cases,  $0.54 \times \theta_2 < \theta_1 \leq (0.97 \times \theta_2)$  in 4/78 cases, and  $\theta_1 \leq 0.54 \times \theta_2$  in 3/78 cases. Ninety-one cases had a pathological diagnosis of the tubule-forming type:  $(0.97 \times \theta_2) < \theta_1$  in 6/91 cases,  $(0.54 \times \theta_2) < \theta_1 \leq (0.97 \times \theta_2)$  in 73/91 cases, and  $\theta_1 \leq (0.54 \times \theta_2)$  in 12/91 cases. Finally, 143 cases had a pathological diagnosis of the scirrhus type:  $(0.97 \times \theta_2) < \theta_1$  in 2/143 cases,  $(0.54 \times \theta_2) < \theta_1 \leq (0.97 \times \theta_2)$  in 14/143 cases, and  $\theta_1 \leq (0.54 \times \theta_2)$  in 127/143 cases. No cases corresponded to other types. The results were similar even when the calculations were performed thrice.

The average variances of  $\theta_2 - \theta_1$  in each pathological class were: The solid type (78):34\_179, the tubule-forming type

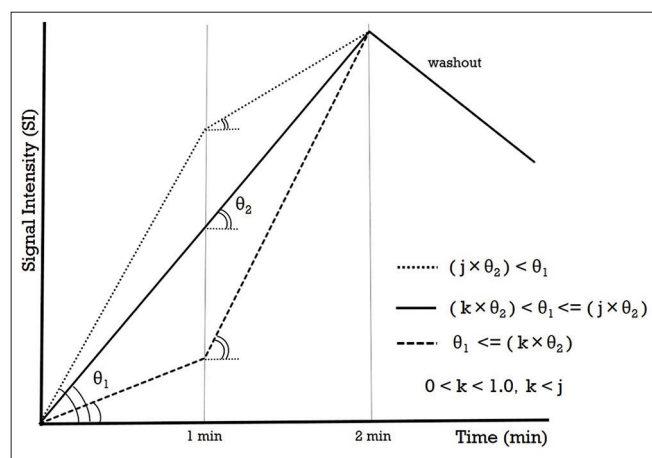


**Figure 4:** Histological classification using time-intensity curve (definition of  $\theta_1$  and  $\theta_2$ ).

(91):14\_113, and the scirrhus type (143):-0.87\_61. The P value by ANOVA was  $1.72 \times 10^{-66}$ , or  $<0.05$ .

### Evaluation of organizational classification using TIC

Based on the results of section 3.1 and assuming that the classification that best matched, the pathological diagnosis was the feature amount of each tissue, the solid type feature amount was  $(0.97 \times \theta_2) < \theta_1$ , the tubule-forming type was  $(0.54 \times \theta_2) < \theta_1 \leq (0.97 \times \theta_2)$ , the scirrhus type was  $\theta_1 \leq (0.54 \times \theta_2)$ , and the discriminant predictive value was 86.9%.

Table 2 shows the sensitivity, specificity, positive reactivity, and negative reactivity for each tissue. The values were

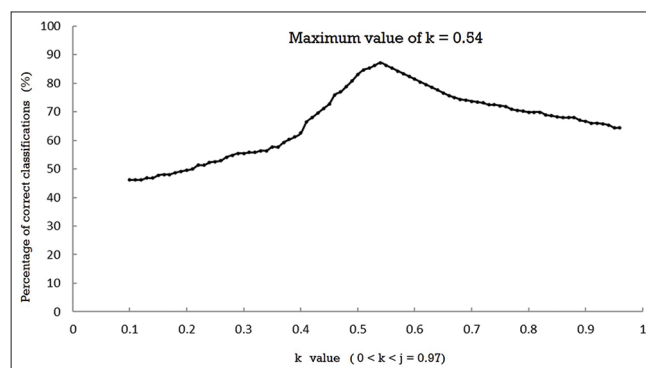


**Figure 5:** Percentage of correct classifications at the values of k and j in the tissue classification formula (1) (j = 0.97) closest to the pathological diagnosis by computer calculation.  $\theta_1 \leq (k \times \theta_2)$ ,  $(k \times \theta_2) < \theta_1 \leq (j \times \theta_2)$ ,  $(j \times \theta_2) < \theta_1$ ; ( $0 < k < 1$ ) (1). There were 312 cases of invasive ductal carcinoma (pathological diagnoses: Solid 78, tubule-forming 91, and scirrhus 143): All women, aged 23–88 years (mean  $57.9 \pm 13.0$  years) and a tumor diameter of 0.7–9.2 cm (mean  $2.4 \pm 2.1$  cm).

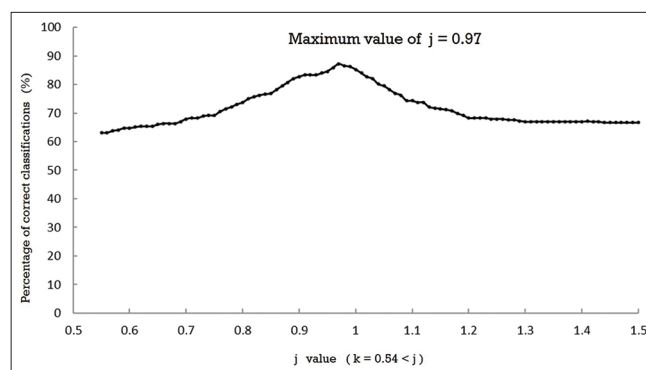


**Figure 6:** Percentage of correct classifications at the values of k and j in the tissue classification formula (1) (k = 0.54) closest to the pathological diagnosis by computer calculation.  $\theta_1 \leq (k \times \theta_2)$ ,  $(k \times \theta_2) < \theta_1 \leq (j \times \theta_2)$ ,  $(j \times \theta_2) < \theta_1$ ; ( $0 < k < 1$ ) (1). There were 312 cases of invasive ductal carcinoma (pathological diagnoses: Solid 78, tubule-forming 91, and scirrhus 143): All women, aged 23–88 years (mean  $57.9 \pm 13.0$  years) and a tumor diameter of 0.7–9.2 cm (mean  $2.4 \pm 2.1$  cm).

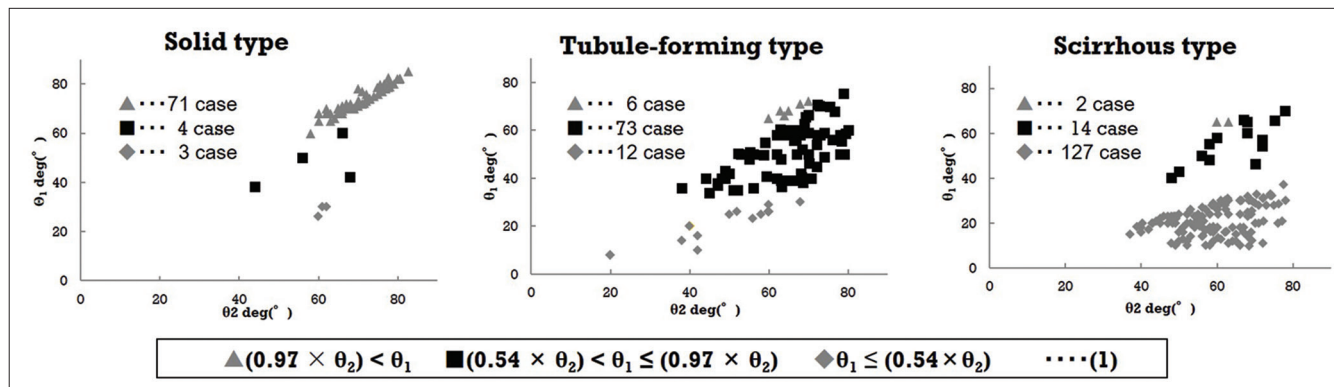


**Figure 7:** Average value of  $\theta_1$  and  $\theta_2$ , as histologically determined by time-intensity curve from each pathological tissue sample. There were 312 cases of invasive ductal carcinoma (pathological diagnoses: Solid 78, tubule-forming 91, and scirrhus 143): All women, aged 23–88 years (mean  $57.9 \pm 13.0$  years) and a tumor diameter of 0.7–9.2 cm (mean  $2.4 \pm 2.1$  cm).

**Table 1:** Tissue classification using time-intensity curve analysis compared with the histopathological results. The pathological diagnoses were: Solid type ( $n=78$ ), tubule-forming type ( $n=91$ ) and scirrhus type ( $n=143$ ). The patients were all women, aged 23–88 years (mean  $57.9 \pm 13.0$  years), with tumor diameters of 0.7–9.2 cm (mean  $2.4 \pm 2.1$  cm).  $n=312$ .

Pathological diagnoses	$(0.97 \times \theta_2) < \theta_1$	$(0.54 \times \theta_2) < \theta_1 \leq (0.97 \times \theta_2)$	$\theta_1 \leq (0.54 \times \theta_2)$
Solid type: 78 cases	71/78	4/78	3/78
Tubule-forming type: 91 cases	6/91	73/91	12/91
Scirrhus type: 143 cases	2/143	14/143	127/143

**Table 2:** Evaluation of tissue classification by time-intensity curve. There were 312 cases of invasive ductal carcinoma (pathological diagnoses: Solid 78, tubule-forming 91, and scirrhus 143): All women, aged 23–88 years (mean  $57.9 \pm 13.0$  years) and a tumor diameter of 0.7–9.2 cm (mean  $2.4 \pm 2.1$  cm) (%).

	Sensitivity	Specificity	Positive predictive value	Negative predictive value	Discriminative predictive value
Solid type	91.0	96.6	89.9	97.0	86.9
Tubule-forming type	80.2	91.9	80.2	91.9	
Scirrhus type	88.8	91.1	89.4	90.6	

91.0%, 96.6%, 89.9%, and 97.0%, respectively, for the solid type; 80.2%, 91.9%, 80.2%, and 91.9%, respectively, for the tubule-forming type; and 88.8%, 91.1%, 89.4%, and 90.6%, respectively, for the scirrhus type.

Figure 8 shows the details of tissue classification using TIC in the same case depicted in Figure 3. Pathological images of 1 pixel ( $0.8 \times 0.6$  mm) at each location, indicated by the TIC classification are shown.

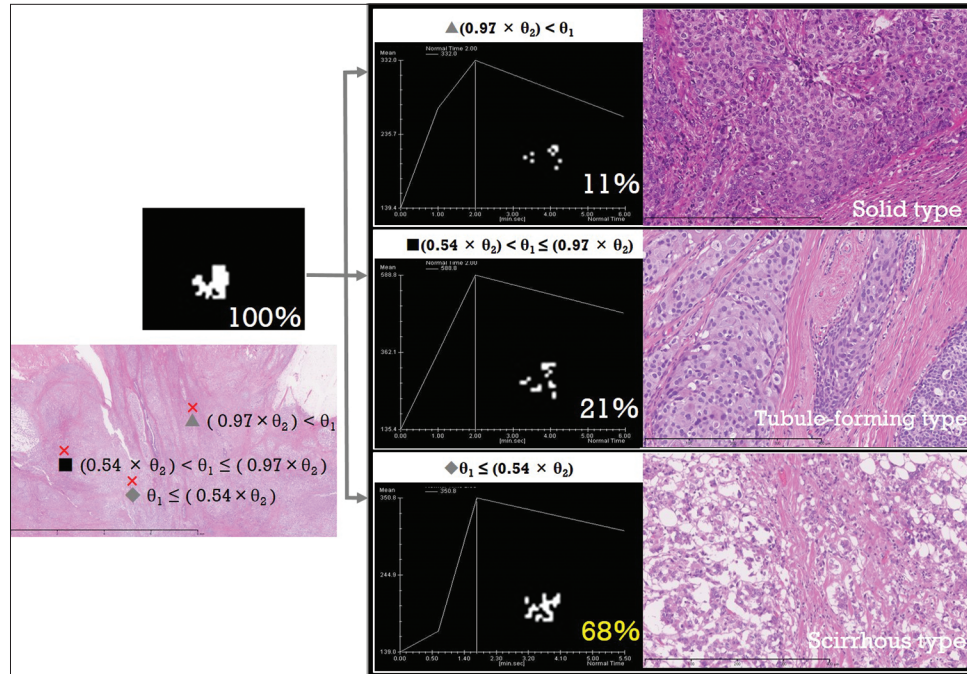
**Comparison of MRI-TIC and ultrasonography**

Table 3 shows the results of tissue classification by MRI-TIC as compared to pathological diagnosis by ultrasonography. For the solid type (78 cases), tubule forming type (91 cases), and scirrhus type (143 cases), the MRI-TIC/ultrasound ratios (including the second extracted diagnosis name) were 71/40, 73/65, and 127/110, respectively. The discriminant

predictive value for MRI-TIC was 86.9% (271/312) and 68.9% (215/312) for the ultrasound.

**DISCUSSION**

In this study, we used an algorithm for classifying the features of the scirrhus, tubule-forming, and solid types of invasive ductal carcinoma by quantitatively analyzing the TIC using mammary gland dynamic MR images; we verified the algorithm in 312 cases. The method described in section 2.2 was used for the tissue classification in TIC, and each feature was clarified from the 312 cases. The angle indicated by the solid type  $(0.97 \times \theta_2) < \theta_1$ , the tubule-forming type  $(0.54 \times \theta_2) < \theta_1 \leq (0.97 \times \theta_2)$ , and the scirrhus type  $\theta_1 \leq (0.54 \times \theta_2)$  was related to the peak time and was similar to the peak time reported by Kamitani *et al.* (solid-tubular carcinoma  $43 \pm 17$  s, papillotubular carcinoma  $47 \pm 19$  s, and scirrhus carcinoma  $63 \pm 24$  s).<sup>[19]</sup> It shows that the peak time



**Figure 8:** Figure 3A depicts the results of histological classification by time-intensity curve and the corresponding pathological images.

**Table 3:** Evaluation of tissue classification (MRI-TIC vs. ultrasound: Same day examination of the same patient). There were 312 cases of invasive ductal carcinoma (pathological diagnoses: Solid 78, tubule-forming 91, and scirrhus 143): All women, aged 23–88 years (mean  $57.9 \pm 13.0$  years) and a tumor diameter of 0.7–9.2 cm (mean  $2.4 \pm 2.1$  cm).  $n=312$ .

Pathological diagnoses	※ <sup>1</sup> MRI-TIC results consistent with pathological diagnosis	※ <sup>2</sup> Ultrasonography results consistent with pathological diagnosis
Solid type: 78 cases	71	40
Tubule-forming type: 91 cases	73	65
Scirrhus type: 143 cases	127	110
Discriminative predictive value	86.9%	68.9%

※<sup>1</sup>MRI-TIC: Magnetic resonance imaging-time intensity curve, ※<sup>2</sup>Ultrasonic diagnosis includes up-to-the-second diagnosis

increases in the order of solid type, tubule-forming type, and scirrhus type. There was a difference in histological construction,<sup>[5-8,15,19]</sup> such that the tubule-forming type was not accompanied by prominent interstitial connective tissue proliferation, the solid type was poor in interstitial connective tissue, whereas the scirrhus type was often accompanied by interstitial connective tissue proliferation. The difference up to the peak time of the contrast medium in this study can be attributed to the difference in histological construction. In other words, it was considered that the difference in the feature amount was related to the difference in the number of tumor cells per unit area (solid type > tubule-forming type > scirrhus type), as observed in the pathological images [Figure 8]. Invasive ductal carcinoma may have mixed histology within 1 lesion. When 2 or more types of histology were found in a pathological diagnosis, the dominant (wide area) tissue was adopted and classified accordingly.<sup>[20]</sup> For this

reason, we classified each pixel in the intratumoral washout portion into 3 TIC features that reflected the tumor tissue type. In addition, the created TIC categories were aggregated to determine the most dominant organizational type. By even quantitatively evaluating the multiple tissue types, the dominant tissue type could be determined.

In addition, there are two reasons why MRI was higher than ultrasonography in terms of the concordance rate with the pathological diagnosis results. The first is that the detection sensitivity of breast cancer is superior, as described in the introduction. The other is that ultrasonography is a unique diagnostic tool in which the result depends greatly on the skills of the operator.<sup>[1]</sup>

In the classification of the histological types in this study, the positive diagnosis rate was 96.0% for the solid type, 89.0% for the tubule-forming type, and 90.1% for the scirrhus type in 312 cases of invasive ductal carcinoma. However,

the TIC-based classification did not completely replicate the pathological diagnosis. The 4 points (pre-phase, injection phase, peak phase, and delay phase) initially collected might explain the discordance. There was a slight difference in the points of the feature quantities  $\theta_1$  and  $\theta_2$  at the strict peak point and 2 minutes after the peak point since finer timed data were not collected.<sup>[10]</sup> This requires future evaluation with a study design accommodating the above points of evaluation.

Another point of significance was that the histologic classification of invasive ductal carcinoma was pathologically determined by observation and was thus subjective rather than objective. It is difficult to observe in entirety all the tissues that become the malignant parts of the lesion, and there is a possibility that the diagnosis results may vary depending on the observer's observational judgments. However, the histological classification of invasive ductal carcinoma according to the present study used scans of all the available imaging data (384 images/case) and extracted the washout part in the tumor so that the results were quantitative and reproducible, eliminating subjectivity and thereby offering an objective and meritorious evaluation.

The histological classification using TIC in this study was consistent with the pathological diagnosis in 86.9% of the 312 cases, thus proving its utility. Moreover, it is considered that 3 factors cause a large difference (15% or more) in the discriminant prediction values between the ultrasonic examination, including the second extraction diagnosis, and this study (MRI-TIC): (1) Ultrasound results depend on the skill of the operator, (2) it is difficult to extract the entire lesion, and (3) it is difficult to quantitatively evaluate the tissue classification.

There are differences in the lymph node metastasis positive rate, 10-year survival rate, etc., depending on the tissue type of invasive ductal carcinoma.<sup>[5,6]</sup> A lot of information is indispensable for the explanation based on the diagnosis and future prediction of the medical condition. At present, we believe that this study can augment pathological evaluation and has great medical utility in the pathological diagnosis in Japan, where the histological type of invasive ductal carcinoma is often specified.

## CONCLUSION

In this study, we classified invasive ductal carcinoma into 3 types – solid, tubule-forming, and scirrhous-based on the features of tumor cell density. This evaluation usually requires a prerequisite diagnosis of invasive ductal carcinoma. Using our method, it is possible to histologically classify the invasive ductal carcinoma. We believe that there is an urgent need for clinical research that improves the accuracy of verification by increasing the number of cases under study, and we hope

the current study contributes and supports the pathological diagnosis.

Quantitative analysis using the TIC of dynamic MRI of the mammary gland is effective for histotyping invasive ductal carcinoma. This method can be used to offer an additional objective dataset for the diagnosis of the histological classification of invasive ductal carcinoma.

## Acknowledgments

We would like to thank Editage ([www.editage.com](http://www.editage.com)) for English language editing. This study has not been presented previously or published as an abstract.

## Declaration of patient consent

Institutional Review Board permission obtained for the study.

## Financial support and sponsorship

Nil.

## Conflicts of interest

There are no conflicts of interest.

## REFERENCES

1. The general rules for clinical and pathological recording of breast cancer. Japanese breast cancer society. *Jap J Surg* 1989;19:612-32.
2. Yerushalmi R, Hayes MM, Gelmon KA. Breast carcinoma-rare types: Review of the literature. *Ann Oncol* 2009;20:1763-70.
3. WHO Classification of Tumours Editorial Board. *Breast Tumours (Medicine)*. 5<sup>th</sup> ed. Lyon: IARC Press; 2019. p. 102-9.
4. Japanese Breast Cancer Society. *General Rules for Clinical and Pathological Recording of Breast Cancer*. 17<sup>th</sup> ed. Tokyo: Kanehara Shuppan; 2012. p. 24-30.
5. Masafumi M, Futoshi A. Invasive ductal carcinoma. *Mod Med Lab J* 2001;32:911-9.
6. Sueyoshi I, Fuminori A. Lymph node metastasis and prognosis of breast cancer tumors 2 cm in diameter or less. *J Jpn Assoc Breast Cancer Screen* 2001;10:239.
7. Kiyoshi N. Status and problems in predicting the histology of breast cancer using imaging diagnosis. *JSCC* 2001;40:505-11. Available from: [https://www.jstage.jst.go.jp/article/jjsc1962/40/5/40\\_5\\_505/\\_pdf](https://www.jstage.jst.go.jp/article/jjsc1962/40/5/40_5_505/_pdf). [Last accessed on 2021 Jan 09].
8. Tohnosu N. Ultrasonic study on breast cancer with special reference to histological type. *Chiba Med J* 1985;61:105-13. Available from: <https://www.opac.ll.chiba-u.jp/da/curator/900042119/kj00004511444.pdf>. [Last accessed on 2021 Jan 09].
9. Berg WA, Gutierrez L, NessAiver MS, Carter WB, Bhargavan M, Lewis RS, *et al.* Diagnostic accuracy of mammography, clinical examination, US, and MR imaging in preoperative assessment

- of breast cancer. *Radiology* 2004;233:830-49.
10. American College of Radiology. ACR BI-RADS ATLAS breast imaging reporting and data system. In: *Magnetic Resonance Imaging*. 5<sup>th</sup> ed. United States: American College of Radiology; 2013. p. 15-9.
  11. Hulka CA, Smith BL, Sgroi DC, Tan L, Edmister WB, Semple JP, *et al.* Benign and malignant breast lesions: Differentiation with echo-planar MR imaging. *Radiology* 1995;197:33-8.
  12. Kuhl CK, Mielcareck P, Klaschik S, Leutner C, Wardelmann E, Gieseke J, *et al.* Dynamic breast MR imaging: Are signal intensity time course data useful for differential diagnosis of enhancing lesions? *Radiology* 1999;211:101-10.
  13. Jansen SA, Fan X, Karczmar GS, Abe H, Schmidt RA, Newstead GM. Differentiation between benign and malignant breast lesions detected by bilateral dynamic contrast-enhanced MRI: A sensitivity and specificity study. *Magn Reson Med* 2008;59:747-54.
  14. Bhooshan N, Giger ML, Jansen SA, Li H, Lan L, Newstead GM. Cancerous breast lesions on dynamic contrast-enhanced MR images: Computerized characterization for image-based prognostic markers. *Radiology* 2010;254:680-90.
  15. Jansen SA, Shimauchi A, Zak L, Fan X, Karczmar GS, Newstead GM. The diverse pathology and kinetics of mass, nonmass, and focus enhancement on MR imaging of the breast. *J Magn Reson Imaging* 2011;33:1382-9.
  16. Agliozzo S, de Luca M, Bracco C, Vignati A, Giannini V, Martincich L, *et al.* Computer-aided diagnosis for dynamic contrast-enhanced breast MRI of mass-like lesions using a multiparametric model combining a selection of morphological, kinetic, and spatiotemporal features. *Med Phys* 2012;39:1704-15.
  17. Mann RM, Mus RD, van Zelst J, Geppert C, Karssemeijer N, Platel B. A novel approach to contrast-enhanced breast magnetic resonance imaging for screening: High-resolution ultrafast dynamic imaging. *Invest Radiol* 2014;49:579-85.
  18. Abe H, Mori N, Tsuchiya K, Schacht DV, Pineda FD, Jiang Y, *et al.* Kinetic analysis of benign and malignant breast lesions with ultrafast dynamic contrast-enhanced MRI: Comparison with standard kinetic assessment. *AJR Am J Roentgenol* 2016;207:1159-66.
  19. Kamitani T, Noguchi T, Saku M. Dynamic MR mammography. Differences of time-intensity curve among each histology. *Jpn J Breast Cancer* 2003;18:240-5.
  20. Japanese Breast Cancer Society. *General Rules for Clinical and Pathological Recording of Breast Cancer*. 18<sup>th</sup> ed. Tokyo: Kanehara Shuppan; 2018. p. 24-30.
  21. Yoshiaki M, Nobuyuki T, Tomomi T, Kenji S, Yuichiro K, Eriko T, *et al.* Computer-aided detection of metastatic brain tumors in magnetic resonance images. *Jpn J Radiol Technol* 2018;74:251-61.
  22. Kanda Y. Investigation of the freely available easy-to-use software 'EZR' for medical statistics. *Bone Marrow Transplant* 2013;48:452-8.

**How to cite this article:** Miyazaki Y, Tabata N, Kubo Y, Shinozaki K. Utility of tissue classification in invasive ductal carcinoma using dynamic magnetic resonance imaging of the mammary gland. *J Clin Imaging Sci* 2021;11:4.